Mon. Not. R. Astron. Soc. **345,** 705–713 (2003)

A high-velocity ionized outflow and XUV photosphere in the narrow emission line quasar PG1211+143

K. A. Pounds,[1⋆] J. N. Reeves,[1,2] A. R. King,[1] K. L. Page,[1] P. T. O'Brien[1] and M. J. L. Turner[1]

[1]*Department of Physics and Astronomy, University of Leicester, Leicester LE1 7RH*
[2]*Laboratory for High Energy Astrophysics, NASA Goddard Space Flight Center, Greenbelt, MD 20771, USA*

Accepted 2003 July 8. Received 2003 July 8; in original form 2003 March 27

ABSTRACT

We report on the analysis of a ∼60-ks *XMM–Newton* observation of the bright, narrow emission line quasar PG1211+143. Absorption lines are seen in both European Photon Imaging Camera and Reflection Grating Spectrometer spectra corresponding to H- and He-like ions of Fe, S, Mg, Ne, O, N and C. The observed line energies indicate an ionized outflow velocity of ∼24 000 km s^{-1}. The highest energy lines require a column density of $N_{\rm H} \sim 5 \times 10^{23}$ cm^{-2}, at an ionization parameter of $\log \xi \sim 3.4$. If the origin of this high-velocity outflow lies in matter being driven from the inner disc, then the flow is likely to be optically thick within a radius of ∼130 Schwarzschild radii, providing a natural explanation for the big blue bump (and strong soft X-ray) emission in PG1211+143.

Key words: galaxies: active – galaxies: general – galaxies: individual: PG1211+143 – galaxies: Seyfert – X-rays: galaxies.

1 INTRODUCTION

One of the most striking recent developments in X-ray studies of active galactic nuclei (AGN) has been the observation, from high-resolution grating spectra obtained with *Chandra* and *XMM–Newton*, of complex absorption indicating circumnuclear (often outflowing) matter existing in a wide range of ionization states (e.g. Sako et al. 2001; Kaspi et al. 2002). Until recently, however, it has generally been assumed that this so-called 'warm absorber' was essentially transparent in the 'Fe K spectral band' above ∼6 keV, with fluorescent line emission from the accretion disc being the main feature in AGN spectra at those energies (e.g. Reynolds & Nowak 2003).

In this paper we report on the spectral analysis of a ∼60-ks *XMM–Newton* observation of the bright quasar PG1211+143. At a redshift $z = 0.0809$ (Marziani et al. 1996) PG1211+143 has a typical X-ray luminosity (2–10 keV) of $\sim 10^{44}$ erg s^{-1}, for $H_0 = 75$ km s^{-1} Mpc^{-1}. The Galactic absorption column towards PG1211+143 is $N_{\rm H} = 2.85 \times 10^{20}$ cm^{-2} (Murphy et al. 1996), rendering it visible over the whole (∼0.2–12 keV) spectral band of the European Photon Imaging Camera (EPIC) and Reflection Grating Spectrometer (RGS) instruments on *XMM–Newton*.

PG1211+143 is a low redshift, optically bright quasar, with a strong 'big blue bump' (BBB). It is unusual in the PG sample of bright quasars in having relatively narrow permitted optical emission lines (Boroson & Green 1992; Kaspi et al. 2000). PG1211+143 was first detected in the X-ray band by *Einstein*, which found a steep spectrum in the ∼0.2–2 keV band (Bechtold et al. 1987; Elvis et al. 1991). A subsequent analysis by Saxton et al. (1993), which combined *EXOSAT* and *GINGA* data, resolved a strong soft X-ray 'excess' above a harder power-law component of photon index $\Gamma \sim 2.1$. An early *ASCA* observation showed the soft excess to be variable, indicating a source region of $\leqslant 10^{15}$ cm (Yaqoob et al. 1994). The improved spectral resolution of *ASCA* further refined the broad-band X-ray description of PG1211+143 (Reeves et al. 1997), with evidence for a broad Fe K emission line [equivalent width (EW) ∼400–750 eV] at ∼6.4 keV. A more recent study of the overall (infrared to X-ray) spectrum of PG1211+143 has been published by Janiuk, Czerny & Madejski (2001), considering in particular the strong emission in the ultraviolet (UV) and soft X-ray bands and proposing its origin in a warm optically thick 'skin' on the accretion disc. This work also included an analysis of an extended *RXTE* observation in 1997, suggesting a cold reflection factor $R = \Omega/2\pi$, where Ω is the solid angle subtended by the reflecting matter, of order unity.

2 OBSERVATION AND DATA REDUCTION

PG1211+143 was observed by *XMM–Newton* on 2001 June 15 yielding a useful exposure of ∼60 ks. In this paper we use data from the EPIC pn camera (Strüder et al. 2001), which has the best sensitivity of any instrument flown to date in the ∼6–10 keV spectral band, the combined EPIC MOS cameras (Turner et al. 2001), and

⋆E-mail: kap@star.le.ac.uk

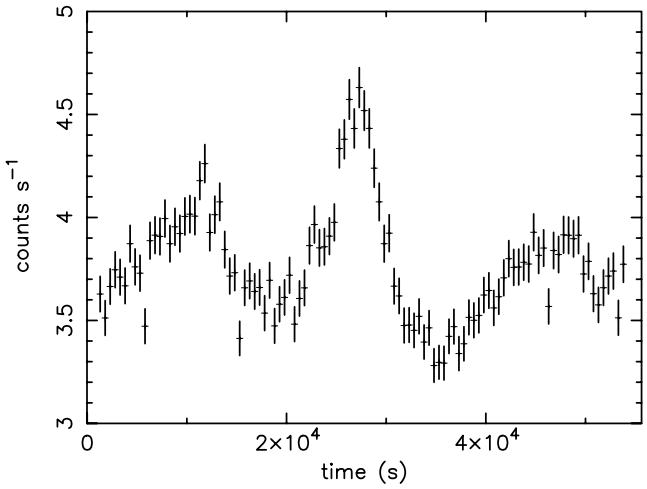

Figure 1. X-ray light curve at 0.2–10 keV from the *XMM–Newton* pn observation of PG1211+143 on 2001 June 15.

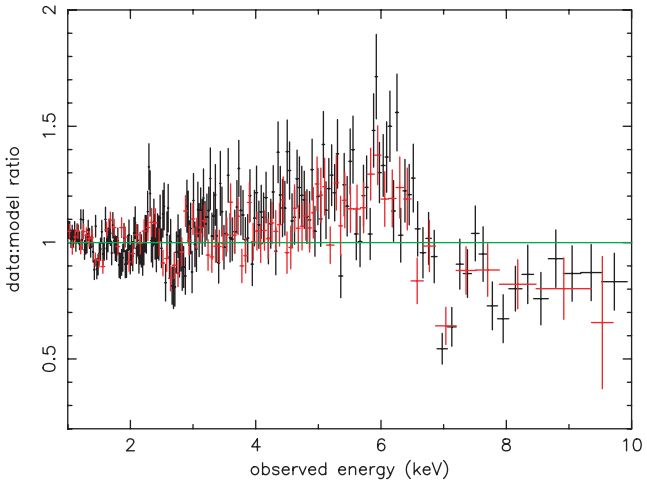

Figure 2. Ratio of the EPIC pn (black) and MOS (red) spectral data to a simple power-law model fitted between 1–10 keV for PG1211+143. The plot shows a broad excess at 3–7 keV and several absorption features including a deep narrow absorption line near 7 keV.

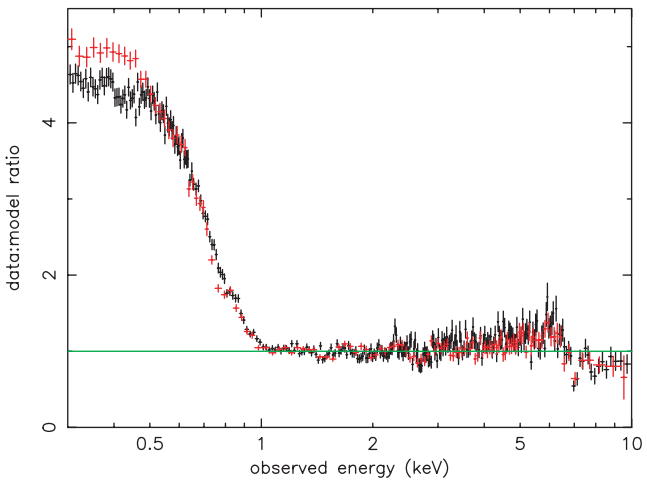

Figure 3. Extension to 0.3 keV of the 1–10 keV power-law model fits for the pn (black) and MOS (red) spectral data, showing the strong soft excess in PG1211+143.

the RGS (den Herder et al. 2001). Reference to the Optical Monitor (Mason et al. 2001) confirmed that the strong optical and UV emission was close to the typical level in PG1211+143. All X-ray data were first screened with the *XMM* Science Analysis System (SAS) v5.3 software and events corresponding to patterns 0–4 (single and double pixel events) were selected for the pn data and patterns 0–12 for MOS1 and MOS2, the latter then being combined. A low-energy cut of 200 eV was applied to all X-ray data and known hot or bad pixels were removed. We extracted source counts within a circular region of 45 arcsec rad defined around the centroid position of PG1211+143, with the background being taken from a similar region, offset from but close to the source. The 0.2–10 keV X-ray pn light curve is reproduced as Fig. 1 and shows ∼30 per cent flux changes over ∼6 ks, similar to those seen in the *ASCA* data. Individual spectra were binned to a minimum of 20 counts per bin, to facilitate use of the χ^2 minimalization technique in spectral fitting. Response functions for spectral fitting to the RGS data were generated from the SAS v5.3.

Spectral fitting was based on the XSPEC package (Arnaud 1996) and used a grid of ionized absorber models calculated with the XSTAR code (Kallman et al. 1996). All spectral fits include absorption due to the line-of-sight Galactic column of $N_{\rm H} = 2.85 \times 10^{20}$ cm^{-2}. Errors are quoted at the 90 per cent confidence level ($\Delta\chi^2 = 2.7$ for one interesting parameter).

3 1–10 keV SPECTRUM

3.1 Power law

X-ray spectra of AGN at 2–10 keV are well fitted, to first order, with a power law of photon index Γ in the range ∼1.6–2 for most radio-quiet AGN, with a fraction (e.g. NLS1) having steeper indices. The widely held view is that this 'hard' X-ray continuum in Seyfert galaxies arises by Comptonization of thermal emission from the accretion disc in a 'hot' corona (e.g. Haardt & Maraschi 1991), and produces additional spectral features by 'reflection' from dense matter in the disc (e.g. Pounds et al. 1990; Fabian et al. 2000).

We began our analysis of PG1211+143 by confirming that there were no obvious spectral changes with source flux and then we proceeded to fit the *XMM–Newton* pn and MOS data integrated over the full ∼60-ks observation. A simple power-law fit over the 1–10 keV band yielded a photon index of $\Gamma \sim 1.79$ (pn) and $\Gamma \sim 1.71$ (MOS), with a broad excess in the data:model ratio between 3–7 keV, and evidence of absorption at higher energies in both data sets (Fig. 2). The fit was statistically unacceptable with an overall χ^2/dof of 1541/1176. When extrapolated to 0.3 keV, the 1–10 keV fits to both pn and MOS data revealed a strong 'soft excess' (Fig. 3).

3.2 Fe K emission and absorption features

To improve the 1–10 keV fit we added further spectral components to match the most obvious features in the data. The indication of an extreme broad emission line suggested reflection from the inner accretion disc, conventionally modelled with a LAOR line in XSPEC (Laor 1991). The addition of a LAOR line, with inclination initially fixed at 30° and $R_{\rm out} = 50R_{\rm s}$ (where $R_{\rm s} = 2GM/c^2$ is the Schwarzschild radius for mass M), resulted in a significant statistical improvement (χ^2/dof of 1304/1172), but with an unrealistically large EW of ∼1.4 keV (pn) and ∼1.1 keV (MOS). To better fit the broad line profile we added a Gaussian line with energy tied to that

of the LAOR line. (Physically, such a Gaussian line could represent emission from larger radii on the disc.) This addition gave a further improvement in the fit, to χ^2/dof of 1278/1167. The LAOR line still had a high EW ∼0.6–0.9 keV, with disc emissivity index $\beta \sim 3.5$, and inner radius $R_{\rm in} \sim 0.75 R_{\rm s}$. The Gaussian emission line component had an rms width $\sigma = 0.28 \pm 0.15$ keV and EW = 0.25 ± 0.11 keV. The (poorly constrained) joint line energy was ∼6.2 keV, or ∼6.7 keV in the source rest frame, implying reflection from highly ionized matter.

We then attempted to fit the narrow absorption features visible in Fig. 2, initially with Gaussian shaped absorption lines in XSPEC. Adding a Gaussian line with energy, width and EW free gave a significantly better fit to the absorption near 7 keV than an absorption edge. The observed line energy was 7.02 ± 0.03 keV, with an rms width of $\leqslant$100 eV, and an EW of 95 ± 20 eV. The addition of this Gaussian absorption line improved the fit to χ^2/dof = 1246/1164. The most likely identifications of this line are Lyα of Fe XXVI or the primary 1s–2p resonance transition in He-like Fe XXV. The rest energies of these lines are separated by 0.26 keV, which would be resolved (or at least produce a broad line) in the EPIC data. The narrowness of the observed feature at ∼7 keV suggests the former identification, with any absorption from the Fe XXV line modifying the Fe K emission line. [We recall that evidence for variable line-of-sight absorption superposed on the Fe K emission line has been previously seen in an *XMM–Newton* observation of Mkn 766 (Pounds et al. 2003).]

A second narrow Gaussian line at 7.9 ± 0.04 keV was less significant, reducing χ^2 to 1234 for 1161 dof. In this case, a statistically better fit (χ^2/dof of 1228/1161) was obtained with an absorption edge at ∼7.7 keV, or with a broader line of width $\sigma \sim 0.3$ keV centred at ∼8.05 keV (EW of 45 ± 12 eV). We choose to proceed with the latter, and provisionally identify it with a blend of the Fe XXV 1s–3p line and Fe XXVI Lyβ, while noting other contributions could be from absorption edges of less highly ionized Fe (XVII or higher), inner shell transitions as recently addressed by Palmeri et al. (2002), or Ni K. A higher (outflow) velocity component of the absorption line seen at ∼7 keV is a further possibility. Fig. 2 suggests the presence of other narrow absorption features in the EPIC data, the most significant being at ∼2.7 keV, and near 1.5 keV. Fitting these two features by successively adding Gaussian lines to the model yielded further reductions in χ^2 of, respectively, 26 and 32 for three fewer dof in each case (Fig. 4).

Details of all absorption lines thus identified in the EPIC data are summarized in Table 1. When corrected for the redshift of PG1211+143, each line energy indicates an origin in the same relativistic outflow, with a velocity of ∼24 000 km s^{-1}. The best determined line profile, for the line at ∼7.02 keV, is essentially unresolved, corresponding to a velocity dispersion of $\leqslant$12 000 km s^{-1}. We shall see in Section 3.5 that a tighter line width constraint is obtained from the RGS data.

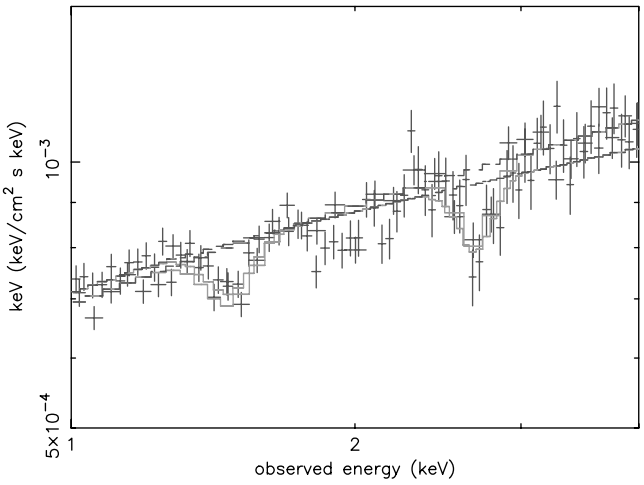

Figure 4. Gaussian absorption line fits to the EPIC pn and MOS data residuals identified with the Lyα lines of S XVI and Mg XII in Table 1. Structure between 1.8–2.2 keV may be related to Si and Au effects in the instrument response. This figure is available in colour in the on-line version of the journal on *Synergy*.

In summary, we find that the 1–10 keV spectrum of PG1211+143 can be described by a broad Fe K emission line, together with absorption features which are best fitted with Gaussian line profiles rather than absorption edges. The proposed identification of these lines, with resonance absorption from highly ionized Fe, S and Mg, indicates an origin in outflowing ionized gas at a velocity of ∼24 000 km s^{-1}.

3.3 An ionized absorber model

To quantify the highly ionized matter responsible for the observed absorption features we then replaced the Gaussian absorption lines in the above model with a grid of photoionized absorbers based on the XSTAR code. These model absorbers cover a wide range of column density and ionization parameter, with outflow (or inflow) velocities as a variable parameter ξ ($=L/nr^2$). All abundant elements from C to Fe are included with the relative abundances as a variable input parameter. In order to limit processing time, the fits assume a fixed width of each absorption line of 1000 km s^{-1} FWHM. An absorber with ionization parameter of $\log \xi \sim 3.4$, and column density of $N_{\rm H} \sim 5 \times 10^{23}$ cm^{-2}, for solar abundances, was found to reproduce the observed absorption lines at ∼7, ∼8 and ∼2.7 keV (Fig. 5), assuming their indicated identifications, and an

Table 1. Absorption lines identified in the parametric fit to the combined EPIC spectrum of PG1211+143. Line energies are in keV. The ionization parameter corresponds to an equal abundance of the emitting and recombining ions.

Line	$E_{\rm obs}$	$E_{\rm source}$	$E_{\rm lab}$	Velocity (km s^{-1})	EW (eV)	$\log \xi$	$\Delta\chi^2$
Fe XXVI Lyα	7.02 ± 0.03	7.59	6.96	24500 ± 1000	95 ± 20	3.8	32
Fe XXV 1s-3p	8.05 ± 0.07	8.70	7.88	24800 ± 1500	45 ± 12	3.2	18
Fe XXVI Lyβ	8.05 ± 0.07	8.70	8.25	23700 ± 1500	45 ± 12	3.8	18
S XVI L-alpha	2.68 ± 0.03	2.89	2.62	24800 ± 1000	32 ± 12	3.0	26
Mg XII L-alpha	1.47 ± 0.03	1.59	1.47	24300 ± 1000	15 ± 6	2.4	32

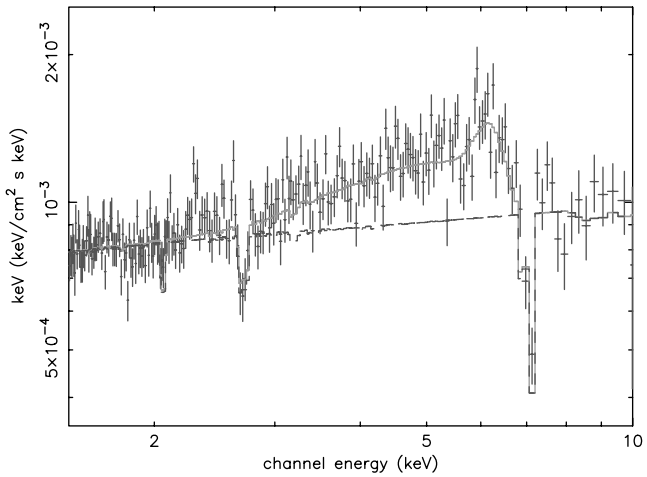

Figure 5. Unfolded spectrum illustrating the XSTAR fit to the *XMM–Newton* observation of PG1211+143 as detailed in Section 3.3. For clarity we only show the pn data. This figure is available in colour in the on-line version of the journal on *Synergy*.

outflow velocity of ∼0.08*c*. We note that most of the uncertainty in the derived column density is on the upside, because allowance for partial covering and saturation in the relatively narrow-line profiles would both increase the above value. The feature attributed to Mg XII was not well modelled by the $\log\xi \sim 3.4$ absorber, indicating the presence of additional absorbing matter at a lower level of ionization. This suggests that corresponding features should be evident in the *XMM–Newton* RGS spectrum. We examine that prediction in Section 3.5.

3.4 Soft excess

Extending the 1–10 keV power-law fits for both pn and MOS spectral data to 0.3 keV shows very clearly (Fig. 3) the strong soft excess first indicated by *Einstein* and *EXOSAT* observations (Elvis et al. 1991; Saxton et al. 1993). In the EPIC data this can be adequately modelled with the addition of blackbody emission components together with two surrogate absorption edges. The parameters for PG1211+143 are a primary blackbody of $kT \sim 110$ eV with a weaker component of $kT \sim 265$ eV, and 'edges' at ∼0.8 and ∼0.98 keV. We note that a similar combination of blackbody emission superimposed by absorption edges has been found previously to be a good parametrization of EPIC spectra of AGN (e.g. Pounds et al. 2003), although – interestingly – in the present case the edge energies are some 10 per cent higher than if associated with the O VII and O VIII edges (at rest). Based on this fit we obtain an average 0.3–10 keV flux for PG1211+143 of 7.5×10^{-12} erg s^{-1} cm^{-2}, corresponding to a luminosity of $\sim 10^{44}$ erg s^{-1} ($H_0 = 75$ km s^{-1} Mpc^{-1}). The blackbody component is dominant in the 0.3–1 keV band, representing ∼75 per cent of the total flux in that band. The 2–10 keV flux was 2.7×10^{-12} erg s^{-1} cm^{-2}, with a corresponding luminosity of 3.3×10^{43} erg s^{-1}.

3.5 Absorption lines in the RGS spectrum

The strongest absorption lines in the EPIC spectrum have been identified with Lyman alpha of Fe XXVI and S XVI. The ionization parameters where these ions and their (recombining) parent ions are in approximate balance are, respectively, $\log\xi \sim 3.8$ and $\log\xi \sim 3.0$, which essentially determines the effective high ionization parameter in the relevant XSTAR fit. The detection of additional absorption in the EPIC data, including an absorption line attributed to Mg XII at 1.47 keV, suggests the ionized outflow includes matter over a range of ionization states, which should be evident in the RGS spectra of PG1211+143. To check this, we began by jointly fitting the RGS-1 and RGS-2 data with a power law and blackbody continuum (from the EPIC fit) and examining the residuals by eye. The most obvious spectral features were found to be in absorption, as is usually the case with Seyfert 1 spectra, a broad line tentatively identified with the forbidden line of O VII (observed at ∼23.8 Å) being the most obvious emission line. A number of weak absorption features are probably due to Fe L shell absorption, but we concentrate here on the relatively unambiguous identifications associated with H- and He-like resonance absorption in C, N, O and Ne, because these offer a direct confirmation of the ionized outflow seen in the EPIC spectrum. Figs 6–9 show the combined RGS1 and RGS2 spectra with the best-fitting XSTAR model superimposed. We retained the high ionization absorber fitted to the EPIC data in the XSTAR model, and added an intermediate ionization component to better reproduce the observed absorption in C, N, O and Ne. A third, low ionization component was added to match the Fe L edge near 17 Å. The best-fitting parameters of this model were:

(1) $N_{\rm H} = 5 \times 10^{23}$ cm^{-2} at an ionization parameter of $\log\xi \sim 3.4$;
(2) $N_{\rm H} = 6 \times 10^{21}$ cm^{-2} at an ionization parameter of $\log\xi \sim 1.7$;
(3) $N_{\rm H} = 8 \times 10^{22}$ cm^{-2} at an ionization parameter of $\log\xi \sim -0.9$.

Importantly, a large outflow velocity was confirmed from this fit with both of the highly ionized components yielding a velocity of ∼24 000 km s^{-1}. The ionization parameters at which each detected ion has a similar abundance to its parent ion in a photoionized plasma are listed in Tables 1 and 2 (Kallman & McCray 1982), and are seen to span the range from $\log\xi = 1.7$–2.2, close to the second outflow component in our XSTAR model fit. Clearly, a single zone photoionized absorber is unable to explain both EPIC and RGS spectra, and the consistent outflow velocities suggest that a more complex ionization structure may be due to density variations across the flow.

A visual examination of the RGS spectrum was then carried out to determine the individual line energies, check the line identifications, and hence the deduced outflow velocities. Although quite deep, the individual line profiles are not very well determined due to the limited statistics in the PG1211+143 data, and this is reflected in the estimated uncertainty in the line EWs. Nevertheless, we conclude there is no doubt on the identification of the listed lines and their consistent 'blueshift'. The results of this visual check, summarized in Table 2, yield a weighted mean outflow velocity of 23 400 km s^{-1}. As noted above, the individual line profiles are not well determined, but are clearly narrow. A 'combined' Lyman alpha profile from the RGS data, shown in Fig. 10, confirms the lines to be remarkably narrow, with a measured FWHM of ∼2000 km s^{-1}, or $\leqslant$1000 km s^{-1} after allowing for the RGS resolution. A comparison with the measured outflow velocity suggests that the material is streaming outward with relatively little turbulence, and that we are viewing down (rather than across) the flow.

The only obvious emission feature in the RGS spectrum, observed at ∼23.8 A ($\lambda_{\rm lab} = 22.1$ A), is most likely due to O VII forbidden line emission dispersed across the outflow. Unlike the absorption lines, this line is resolved in the RGS data, with FWHM ∼6000 km s^{-1}. The measured EW is 165 ± 30 mA, a part of which may be due to

O VII resonance and intercombination line emission. Interestingly, the observed flux in the O VII emission line (6×10^{-5} photon s^{-1} cm^{-2}) is ∼2.5 times greater than that in the O VII resonance absorption line. As noted elsewhere, the latter may be saturated in the core of the line, but the strength of the emission line strongly suggests that the outflow has a large covering factor, i.e. the cone angle is wide. The measured profile and low projected outflow velocity for the O VII emission line gives further support to such a geometry for the outflow. Assuming $T_e \sim 10^6$ K, and a recombination coefficient (to O VII) of $\sim 10^{-12}$ cm^3 s^{-1} (Verner & Ferland 1996), the observed O VII emission corresponds to an emission measure (n^2V) of 1.2×10^{55} cm^{-3} for a solar abundance of oxygen. Combining this emission measure with the line-of-sight column density ($n\delta r$) $\sim 10^{24}$ cm^{-2} allows us to estimate the radius of a hemispherical outflow $\sim 3 \times 10^{15}$ cm, with $n \sim 3 \times 10^8$ cm^{-3}.

4 DISCUSSION

Analysis of the *XMM–Newton* observation of PG1211+143 has revealed several remarkable features.

The unusually strong soft excess indicated in previous observations is confirmed. The dominance of this component below ∼1 keV suggests an origin as intrinsic thermal emission from the accretion disc, although it has long been known that the temperature of a standard 'thin disc' is too low in AGN to radiate strongly in the X-ray band. Comptonization of cooler disc photons in a warm 'skin' on the disc surface has previously been invoked as an explanation of the soft X-ray excess in PG1211+143 (e.g. Janiuk et al. 2001), while Bechtold et al. (1987) first suggested that the soft X-ray flux was a physical extension of the BBB bump, which is particularly strong in PG1211+143 and contains much of the bolometric luminosity. We suggest, in Section 4.2, that this dominant 'thermal emission' is a natural consequence of the high-density outflow.

A second notable feature in the EPIC spectrum is the broad Fe K line emission, exhibiting an extreme 'red wing'. We note that the extreme parameters of this emission line, including the EW, are reduced (but not removed) when absorption visible in the 7–10 keV band is accounted for. We suggest a possible alternative to the 'relativistic' Fe K emission line in Section 4.3.

The most interesting revelation in the *XMM–Newton* observation of PG1211+143 is the discovery of an absorption line structure, in both EPIC and RGS data, indicating a high column, high ionization absorber outflowing at a velocity of ∼24 000 km s^{-1}. The remarkable agreement of the implied velocities from a wide range of absorption lines leaves little doubt that they have a common origin, although the coexistence of ions with ionization energies as disparate as Fe XXVI and C VI implies a range of ionization parameter. Although the coincidence of the measured outflow with the redshift of PG1211+143 is also remarkable, and we note that PG1211+143 is viewed through the Magellanic Stream and the Virgo Cluster (e.g. Impey, Petry & Flint 1999), the presence of a large column density of highly ionized gas in either location would be a major surprise. The detection of O VII emission at a velocity closer to the systemic velocity of PG1211+143 further supports the ionized matter being intrinsic to the AGN. For the remainder of this paper we therefore continue to consider our results in terms of absorption in PG1211+143.

4.1 A high velocity ionized outflow

Previous high-resolution X-ray spectra of Seyfert 1 galaxies have found evidence for a broad range of (low to moderate) ionization states and outflow velocities of typically 100–1000 km s^{-1}. The long *Chandra* exposure of the Seyfert galaxy NGC 3783 is a template of such studies (Kaspi et al. 2002). However, until now, any absorption in the Fe K band (above ∼7 keV) has generally been attributed to continuum (edge) absorption associated with reflection from the accretion disc. A recent exception was the report of an absorption feature in the X-ray spectrum of a high-redshift BAL quasar (APM 08279+5255), which has been alternatively identified with the absorption edge of Fe XV–XVIII (Hasinger, Schartel & Komossa 2002), or with strongly blueshifted resonance absorption lines of Fe XXV or XXVI (Chartas et al. 2002). An earlier *ASCA* observation also found evidence for an 'absorption line' superimposed on the 'red wing' of a broad Fe K emission line in the Seyfert galaxy NGC 3516 (Nandra et al. 1999). The question remains whether highly ionized gas capable of imparting Fe K absorption features on AGN spectra is a significant component in the outflow of many AGN, and is simply remaining undetected due to the poor sensitivity of current observations of AGN spectra above ∼7 keV. In the latter respect, it may be instructive to note that ionized resonance absorption lines of Fe XXV and XXVI have been seen in the *Chandra* HETGS spectrum of the (much brighter) microquasar GRS 1915+105 (Lee et al. 2002).

An important aspect of our present observations is that the column density of the most highly ionized matter in the line of sight is high. In the case of PG1211+143 we find an equivalent hydrogen column (assuming solar abundances) approaching 10^{24} cm^{-2}. Although the geometry of the outflow is unknown, it is a reasonable expectation that near its source the flow is optically thick. The interesting consequence, which we note in Section 4.2, is that the outflow predicts an inner 'photosphere' which is then a natural source of a major part of the radiated luminosity (BBB to soft X-ray emission) of PG1211+143.

Other important implications following from the detection of a high column, high velocity outflow in PG1211+143 are a mass loss and kinetic energy comparable to the accreting mass and the bolometric luminosity. For the observed Fe XXVI absorption line $\log \xi \sim 3.8$ (Table 1) where $\xi = L/nr^2$. With an ionizing X-ray luminosity ($\gtrsim$7 keV) of 3×10^{43} we can estimate nr^2 to be $\sim 5 \times 10^{39}$ cm^{-1}. Assuming a spherically symmetric flow, at an outflow velocity of $0.08c$, the mass-loss rate is then of the order of $\sim 3.5b\,M_\odot$ yr^{-1}, where $b \leqslant 1$ allows for the collimation of the flow. Assuming the measured outflow velocity is the same as the launch velocity (i.e. the material is then 'coasting'), the associated kinetic energy is $6.5b \times 10^{44}$ erg s^{-1}.

4.2 An XUV photosphere

The previous subsection shows that the column density of the outflow seen in PG1211+143 is close to being optically thick in the continuum. In fact, this is inevitable if the mass outflow rate is comparable to the accretion rate required to power radiation at the Eddington limit.

We assume that the outflow quickly reaches a terminal velocity v and thereafter coasts. Then mass conservation shows that the outflow density is

$$\rho = \frac{\dot{M}}{4\pi v b r^2} \tag{1}$$

at radius r, where $\dot{M}$ is the mass-loss rate. The electron scattering optical depth through the outflow, viewed from infinity down to radius R, is

$$\tau = \int_R^\infty \kappa\rho \, \mathrm{d}r = \frac{\kappa \dot{M}}{4\pi v b R} \tag{2}$$

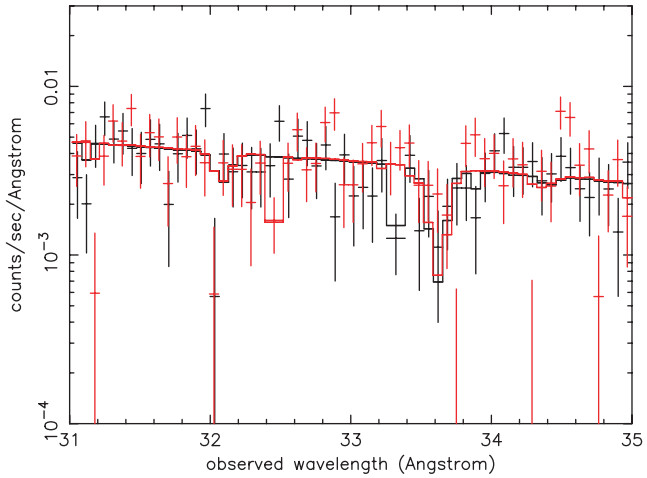

Figure 6. RGS spectrum from 31–35 Å fitted with the photoionized model described in Section 3.5. The C VI Lyα absorption line is observed at 33.62 Å.

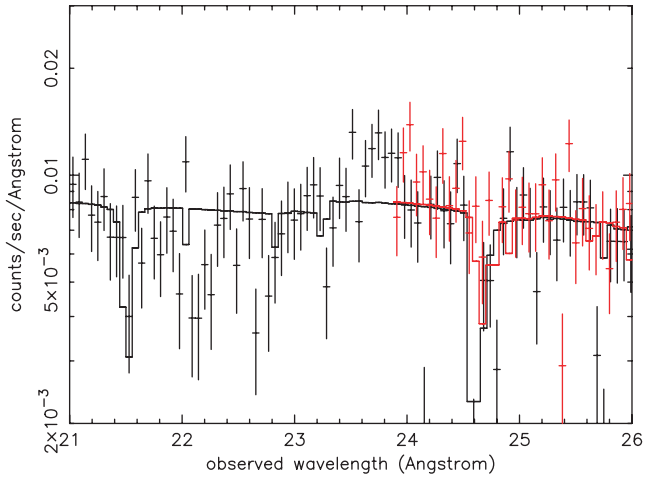

Figure 7. RGS spectrum from 21–26 Å showing resonance absorption lines at 21.55 Å (O VII 1s–2p) and 24.78 Å (N VII Lyα). The relatively strong absorption feature at ∼22.1 A is not identified but may be a blend of the O VII intercombination line pair and the O VI 1s–2p inner shell transition. A broad emission feature at ∼23.8 Å is identified with the O VII forbidden line.

where $\kappa \simeq \sigma_{\rm T}/m_{\rm H}$ is the opacity. The Eddington accretion rate is

$$\dot{M}_{\rm Edd} = \frac{4\pi G M}{\eta \kappa c} \tag{3}$$

where ηc^2 is the accretion yield from unit mass. Combining these equations then gives

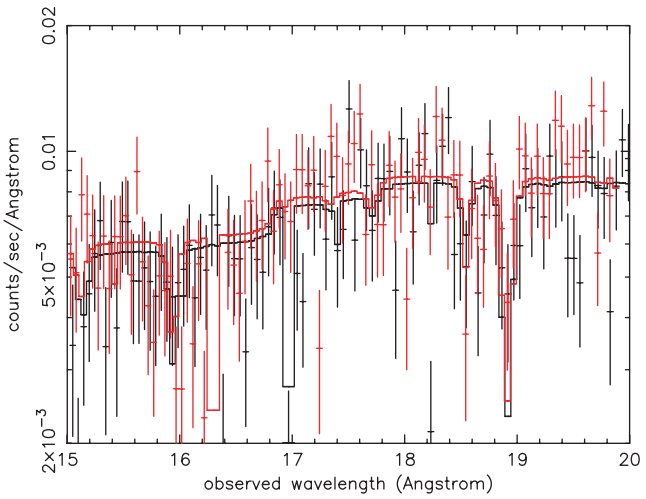

Figure 8. RGS spectrum from 15–20 Å showing resonance absorption lines at 18.90 Å (O VIII Lyα), 18.60 Å (O VII 1s–3p) and 15.98 Å (O VIII Lyβ).

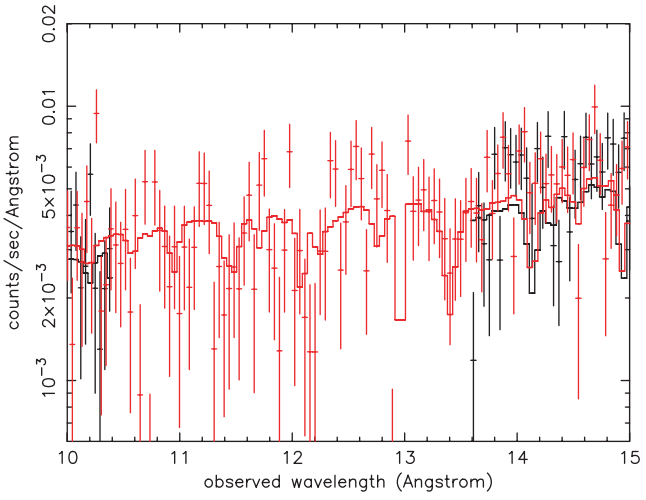

Figure 9. RGS spectrum from 10–15 Å showing absorption lines at 13.40 Å (Ne IX 1s–2p) and 12.17 Å (Ne X Lyα). Several Fe L lines are also indicated and we note that both Ne lines are probably blended with lines of Fe XVII–XXI, limiting their present value in characterizing the outflow from PG1211+143.

$$\tau = \frac{1}{2\eta b}\frac{R_{\rm s}}{R}\frac{c}{v}\frac{\dot{M}}{\dot{M}_{\rm Edd}} \tag{4}$$

where $R_{\rm s} = 2GM/c^2$ is the Schwarzschild radius for mass M. Defining the photospheric radius $R_{\rm ph}$ as the point where $\tau = 1$ gives

Table 2. Absorption lines identified in the RGS spectrum of PG1211+143. All wavelengths are in angstroms. The ionization parameter corresponds to equal abundance of the emitting and recombining ions.

Line	$\lambda_{\rm obs}$	$\lambda_{\rm source}$	$\lambda_{\rm lab}$	Velocity (km s^{-1})	EW (mA)	log ξ
Ne X Lyα	12.07 ± 0.03	11.17	12.13	23700 ± 800	50 ± 20	2.2
Ne IX 1s-2p	13.40 ± 0.05	12.40	13.45	23400 ± 1100	70 ± 15	1.8
O VIII Lyβ	15.98 ± 0.07	14.78	16.01	23000 ± 1300	60 ± 25	1.9
O VIII Lyα	18.90 ± 0.03	17.49	18.97	23400 ± 470	120 ± 25	1.9
O VII 1s-2p	21.55 ± 0.05	19.94	21.60	23100 ± 700	60 ± 15	1.7
O VII 1s-3p	18.60 ± 0.05	17.21	18.63	22900 ± 810	25 ± 10	1.7
N VII Lyα	24.78 ± 0.03	22.93	24.78	22400 ± 360	50 ± 10	1.8
C VI Lyα	33.62 ± 0.03	31.10	33.72	23300 ± 270	90 ± 25	1.7

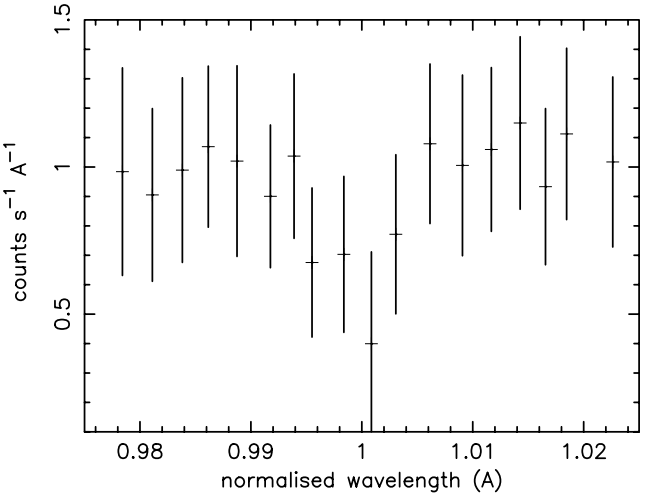

Figure 10. A composite profile of the Lyα lines of C VI, N VII, O VIII and Ne X showing the relatively narrow line width discussed in Section 3.5.

$$\frac{R_{\rm ph}}{R_{\rm s}} = \frac{1}{2\eta b}\frac{c}{v}\frac{\dot{M}}{\dot{M}_{\rm Edd}} \simeq \frac{5}{b}\frac{c}{v}\frac{\dot{M}}{\dot{M}_{\rm Edd}} \quad (5)$$

where we have taken $\eta \simeq 0.1$ at the last step. Because $b \leqslant 1$, $v/c < 1$ we see that $R_{\rm ph} > R_{\rm s}$ for any outflow rate $\dot{M}$ of the order of $\dot{M}_{\rm Edd}$. In other words, any black hole source accreting above the Eddington limit is likely to have a scattering photosphere at several tens of $R_{\rm s}$. This fact is exploited by Mukai et al. (2003) and Fabbiano et al. (2003) in interpreting bright supersoft sources (including supersoft ultraluminous X-ray sources), and is explored in more detail in a companion paper (King & Pounds 2003).

Because a scattering optical depth τ degrades photons of energy $\gtrsim 500\tau^{-2}$ keV we note that the observed hard X-ray flux must be emitted at radii $r \gtrsim R_{\rm s}$, and suggest shocks in the outflow as a promising candidate. This limits the medium-energy X-ray luminosity to a fraction of the outflow kinetic energy $\dot{M}v^2/2$, a constraint easily satisfied for PG1211+143.

In PG1211+143 we estimate $\dot{M}/b \sim 3.5\,{\rm M}_\odot\ {\rm yr}^{-1}$. With $\dot{M}_{\rm Edd} = 1.6\ {\rm M}_\odot\ {\rm yr}^{-1}$, appropriate for a non-rotating supermassive black hole (SMBH) of $M = 4 \times 10^7\ {\rm M}_\odot$ (Kaspi et al. 2000), we find $R_{\rm ph} \simeq 130 R_{\rm s}$ or $\sim 10^{15}$ cm. A wide angle outflow is indicated by the strength and low projected velocity of the O VII emission line (Section 4.1), corresponding to case 1 in King & Pounds (2003), where the flow geometry limits the leakage of photons from the side of the cone. For PG1211+143 we therefore assume a value of $b \sim 0.8$, which then yields an outflow mass rate of $\dot{M} \sim 3\ {\rm M}_\odot\ {\rm yr}^{-1}$, and a kinetic energy $\sim 5 \times 10^{44}$ erg s^{-1}. This is clearly adequate to power a large fraction of the medium-energy X-ray luminosity $\sim 10^{44}$ erg s^{-1}

The scattering photosphere discussed above must be larger than the thermalization region where true absorption dominates and the soft thermal continuum (BBB) is formed. This implies an effective blackbody temperature $\gtrsim 6 \times 10^4$ K for a luminosity of 4×10^{45} erg s^{-1}, broadly consistent with the strong BBB continuum which dominates the bolometric luminosity of PG1211+143.

4.3 The relativistic Fe K emission line

An important question raised by the existence of an optically thick photosphere above the inner accretion disc is how the relativistic Fe K line could be seen, if the innermost accretion disc is obscured. However, the detection of a large column density of highly ionized matter in the line of sight to the hard X-ray source suggests that the extreme 'red wing', evident between ~3–6 keV in a simple power-law fit to PG1211+143, may actually be an artefact of absorption by more moderately ionized gas partially covering the X-ray source. Fig. 11 shows such an alternative fit to the 1–10 keV EPIC spectrum of PG1211+143. This fit, with $\Gamma \sim 2.04$, retains the highly ionized outflow required to model the observed absorption lines, but now includes a second component, of column density 2×10^{23} cm^{-2} and ionization parameter $\log \xi \sim 0.5$, with a covering factor of ~0.42. The statistical quality of this fit is comparable to that including the LAOR line described in Section 3.2. The fit does still require an Fe K emission line, now described by a Gaussian profile with $\sigma \sim 120$ eV and EW ~ 240 eV, at an observed mean energy of ~6.0 keV (~6.5 keV in the rest frame). We note that this emission could arise by reflection from ionized matter in the unobscured disc, but could also include a significant component via re-emission from ionized gas in the outflow.

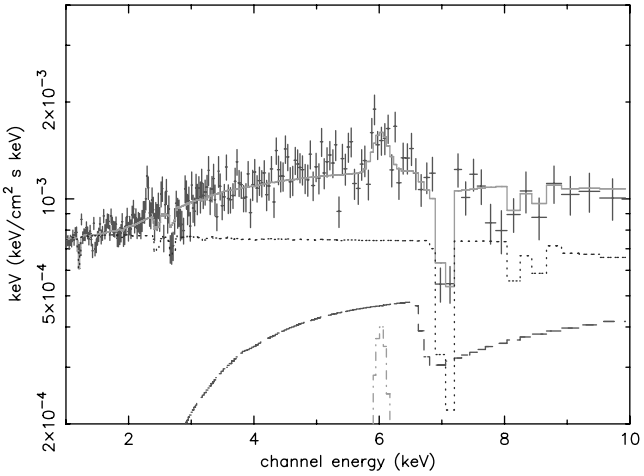

Figure 11. Unfolded spectrum of PG1211+143 modelled at 1–10 keV with a power law, Gaussian emission line and highly ionized outflow. The addition of a second, lower ionization absorber covering ~0.45 of the hard X-ray source replaces the relativistic broad Fe K of earlier fits. This figure is available in colour in the on-line version of the journal on *Synergy*.

4.4 The X-ray spectrum of PG1211+143, a high accretion rate AGN

The average 0.3–10 keV band luminosity of PG1211+143 during our *XMM–Newton* observation was $\sim 10^{44}$ erg s^{-1}. A simultaneous observation with the Optical Monitor on *XMM–Newton* (Mason et al. 2001) showed the energetically dominant BBB to be at a typical value, with a bolometric luminosity of the order of 4×10^{45} erg s^{-1}. Together with the reverberation mass estimate for the SMBH in PG1211+143 of $\sim 4 \times 10^7\ {\rm M}_\odot$ (Kaspi et al. 2000) this luminosity implies accretion in PG1211+143 at close to the Eddington rate. We have argued previously that a high accretion rate may be the key to the characteristic X-ray properties of narrow-line Seyfert 1 galaxies (e.g. Pounds & Vaughan 2000), and the present observation (of a narrow-line quasar) suggests that a further signature of a high accretion rate may appear as Fe K absorption in a highly ionized and massive outflow.

4.5 Relation to Broad Absorption Line QSOs

Hitherto, most evidence for extreme outflows in AGN has been found in UV studies of BAL quasi-stellar objects (QSOs). The observation reported here, of a massive high velocity outflow from PG1211+143, broadens the scope of such studies. BAL QSOs show absorption in a variety of, mainly high-ionization, UV resonance transitions with velocity widths up to $\sim$30 000 km s^{-1} (e.g. Weymann et al. 1991). About 10 per cent of optically selected QSOs display BALs. As BAL QSOs appear otherwise similar to non-BAL QSOs, an 'orientation model' is traditionally invoked in which BAL QSOs are those in which the particular line of sight intersects an outflow which may be intrinsic to all QSOs. This model has recently been questioned by the discovery of a relatively high fraction (15–20 per cent) of radio-loud BAL quasars in the Very Large Array (VLA) FIRST bright quasar survey (Becker et al. 2000). Becker et al. propose that BAL objects may be young or have recently been fuelled. In any case, the higher fraction of quasars that have BALs implies that a higher fraction of the line of sight to the nucleus is covered with substantial absorbing material.

Determining the amount of gas along the line of sight to a BAL is generally problematic due to a poor understanding of the relation between UV and X-ray absorption and the geometry of the flow. Fitting UV absorption lines suggests $N_{\rm H} \geqslant 10^{22}$ cm^{-2}, whereas the generally weak X-ray fluxes imply columns an order of magnitude or more higher (e.g. Hamann 1998; Sabra & Hamann 2001; Gallagher et al. 2002). Models in which the BAL gas is launched more or less vertically off a disc and then accelerated by radiation pressure (Murray et al. 1995; Proga, Stone & Kallman 2000) are reasonably consistent with the UV data but have difficulty in accelerating the large columns of material seen in X-rays unless they are launched from very close to the black hole – as we propose for PG1211+143.

In summary, while PG1211+143 has strong soft X-ray emission and is not a BAL QSO in the UV, it does display a fast moving outflow and a line-of-sight column density which are similar to those required to explain, respectively, the UV and X-ray properties of BAL QSOs. Whether the outflow in PG1211+143 becomes capable of producing BAL features further out in the flow, but we simply do not intersect such a line of sight, is unclear. Neither do we yet know how common are X-ray absorption features as reported here for PG1211+143, nor whether the X-ray absorbing gas causing BAL QSOs to be 'X-ray weak' is in outflow. However, it seems likely that the BAL phenomena and the high velocity outflow in PG1211+143 are closely related.

5 CONCLUSIONS

(1) An *XMM–Newton* observation of the bright quasar PG1211+143 has revealed evidence of a high velocity ionized outflow, with a mass and kinetic energy comparable to the accretion mass and bolometric luminosity, respectively.

(2) A further implication of the high observed column density is that the inner flow is likely to be optically thick, providing a natural explanation for the strong BBB and soft X-ray emission in PG1211+143.

(3) An extreme relativistic Fe K emission line apparent in a simple power-law fit to the data can, alternatively, be explained in terms of partial covering of the continuum source by overlying matter in a lower ionization state.

(4) We suggest that the above properties might be common in AGN accreting at or above the Eddington limit.

ACKNOWLEDGMENTS

The results reported here are based on observations obtained with *XMM–Newton*, a European Space Agency (ESA) science mission with instruments and contributions directly funded by ESA Member States and the USA (NASA). The authors wish to thank the SOC and SSC teams for organizing the *XMM–Newton* observations and initial data reduction and the referee for a careful and constructive reading of the initial text. ARK gratefully acknowledges a Royal Society Wolfson Research Merit Award.

REFERENCES

Arnaud K. A., 1996, in Jacoby G. H., Barnes J., eds, ASP Conf. Ser. Vol. 101, XSPEC: The First Ten Years. Astron. Soc. Pac., San Francisco, p. 17
Bechtold J., Czerny B., Elvis M., Fabbiano G., Green R. F., 1987, ApJ, 314, 699
Becker R. H., White R. L., Gregg M. D., Brotherton M. S., Laurent-Muehleisen S. A., Arav N., 2000, ApJ, 538, 72
Boroson T. A., Green R. F., 1992, ApJS, 80, 109
Chartas G., Brandt W. N., Gallagher S. C., Garmire G. P., 2002, ApJ, 569, 179
den Herder J. W. et al., 2001, A&A, 365, L7
Elvis M., Wilkes B., Giommi P., McDowell J., 1991, ApJ, 378, 537
Fabbiano G., Zezas A., King A. R., Ponman T. J., Rots A., Schweizer F., 2003, ApJ, 584, L5
Fabian A. C., Iwasawa K., Reynolds C. S., Young A. J., 2000, PASP, 112, 1145
Gallagher S. C., Brandt W. N., Chartas G., Garmire G. P., 2002, ApJ, 567, 37
Haardt F., Maraschi L., 1991, ApJ, 350, L81
Hamann F., 1998, ApJ, 500, 798
Hasinger G., Schartel N., Komossa S., 2002, ApJ, 573, L77
Impey C. D., Petry C. E., Flint K. P., 1999, ApJ, 524, 536
Janiuk A., Czerny B., Madejski G. M., 2001, ApJ, 557, 408
Kallman T., McCray R., 1982, ApJS, 50, 263
Kallman T., Liedahl D., Osterheld A., Goldstein W., Kahn S., 1996, ApJ, 465, 994
Kaspi S., Smith P. S., Netzer H., Maoz D., Jannuzi B. T., Giveon U., 2000, ApJ, 533, 631
Kaspi S. et al., 2002, ApJ, 574, 643
King A. R., Pounds K. A., 2003, MNRAS, 345, 657
Laor A., 1991, ApJ, 376, 90
Lee J. C., Reynolds C. S., Remillard R., Shultz N. S., Blackman E. G., Fabian A. C., 2002, ApJ, 567, 1102
Marziani P., Sulentic J. W., Dultzin-Hacyan D., Clavani M., Moles M., 1996, ApJS, 104, 37
Mason K. O. et al., 2001, A&A, 365, L36
Mukai K., Pence W. D., Snowden S. L., Kuntz K. D., 2003, ApJ, 582, 184
Murray N., Chiang J., Grossman S. A., Voit G. M., 1995, ApJ, 451, 498
Murphy E. M., Lockman F. J., Laor A., Elvis M., 1996, ApJS, 105, 369
Nandra K., George I. M., Mushotzky R. F., Turner T. J., Yaqoob T., 1999, ApJ, 523, L17
Palmeri P., Mendoza C., Kallman T. R., Bautista M. A., 2002, ApJ, 577, L119
Pounds K. A., Vaughan S., 2000, NewA Rev., 44, 431
Pounds K. A., Nandra K., Stewart G. C., George I. M., Fabian A. C., 1990, Nat, 344, 132
Pounds K. A., Reeves J. N., Page K. L., Wynn G. A., O'Brien P. T., 2003, MNRAS, 342, 1147
Proga D., Stone J. M., Kallman T. R., 2000, ApJ, 543, 686
Reeves J. N., Turner M. J. L., Ohashi T., Kii T., 1997, MNRAS, 292, 468
Reynolds C. S., Nowak M. A., 2003, Phys. Rep., 377, 389

Sabra B. M., Hamann F., 2001, ApJ, 563, 555
Sako M. et al., 2001, A&A, 365, L168
Saxton R. D., Turner M. J. L., Williams O. R., Stewart G. C., Ohashi T., Kii T., 1993, MNRAS, 262, 63
Strüder L. et al., 2001, A&A, 365, L18
Turner M. J. L. et al., 2001, A&A, 365, L27
Verner D. A., Ferland D. J., 1996, ApJS, 103, 467
Weymann R. J., Morris S. L., Foltz C. B., Hewitt P. C., 1991, ApJ, 373, 23
Yaqoob T., Serlemitsos P., Mushotzky R., Madejski G, Turner T. J., Kunieda H., 1994, PASJ, 46, L173

This paper has been typeset from a TEX/LATEX file prepared by the author.